Corrosion Science 190 (2021) 109661

Contents lists available at ScienceDirect

Corrosion Science

journal homepage: www.elsevier.com/locate/corsci

Optimizing smart self-healing coatings: Investigating the transport of active agents from the coating towards the defect

Yue Yin, Matthias Schulz, Michael Rohwerder *

Max-Planck-Institut für Eisenforschung GmbH, 40237, Düsseldorf, Germany

ARTICLE INFO

Keywords:
Intrinsically Conducting Polymers (ICPs)
Polypyrrole
Ionic transportation
Scanning Kelvin Probe (SKP)
Self-healing coatings
Corrosion protection

ABSTRACT

There are many studies on different concepts for so called smart self-healing coatings providing safe storage and corrosion triggered release of inhibitors. However, achieving an efficient transport of the released inhibitor to the defect is so far a widely neglected issue, although it is crucial for the overall performance. Hence, an in-depth investigation was carried out on inhibitor transport through the coating system into the defect, based on dedicated model sample set-ups. The main focus was on the possible beneficial role of an interfacial polypyrrole layer on the overall performance. Especially for some organic inhibitors huge effects were observed.

1. Introduction

A key difference between Intrinsically Conducting Polymers (ICPs) and conventional non-conducting organic coatings lies in the ability of the former to transport ions automatically through a switch of the redox state from the conductive (half-oxidized) state to the partially reduced state [1–3]. The penetration and transport of ions through the ICP films are associated with weak intermolecular interaction and the absence of a strong physical barrier. Based on this property, ionic mobility and transport play an important role in many applications of ICPs, such as in organic electrochemical transistors [1], separator membranes [4], batteries [5] and biosensors [6]. In this work, however, the focus is on the transport of ions in (partially) reduced ICPs films, as fast transport of active agents is of particular importance for optimizing the overall performance of self-healing coating in the field of corrosion protection, a subject that is currently attracting a great deal of attention. Recently it has been shown that optimized signal spreading can be achieved by the use of an intermediate polypyrrole (PPy) film, applied directly onto the metal surface and beneath the non-conductive coating containing the corrosion inhibitor loaded capsules [7]. The capsules in that latter work were also made from conducting polymer, which has been shown in earlier works to work well in terms of safe storage and efficient corrosion triggered release of corrosion inhibitors and monomers for the formation of a new polymer coating at the defect [8,9].

Concerning improved transport of such active species the work of Uebel et al. indicates that films of conducting polymer directly applied onto the metal, may not only enhance trigger signal spreading, but may also may have a positive effect on transporting corrosion inhibitor to the defect site [7]. To date, relatively little work has been published regarding ion transport through ICPs and its application on corrosion protection. As will be shown in the following, indeed ICPs play a crucial role for designing coating systems with optimized smart self-healing performance also because of the high transport capability for active agents to the defect site.

ICPs are key materials from the point of view of both fundamental research and practical applications. In general, an ICP film is a positive charged polymer backbone in which the positive charge is associated with the according amount of negatively charged dopant anions. The redox reactions of the ICPs are controlled by the insertion or expulsion of counterions [10], and anions as well as cations can be involved in the charge compensation process. Two extreme cases can be considered for the charge compensation during redox transitions: in the one case the counter-anions are highly mobile and the main exchanged species during the redox transitions (see eq. (1) below), in the other case the anions in the ICP are highly immobile and mainly cations are exchanged [11–14] (see Eq. 2):

$$PPy^{+}(A^{-}) + C^{+} + e^{-} \Leftrightarrow PPy^{o} + A^{-} + C^{+} \quad (1)$$

$$PPy^{+}(A^{-}) + C^{+} + e^{-} \Leftrightarrow PPy^{o}(AC) \quad (2)$$

where PPy^{+} and PPy^{o} represent the doped (oxidized) state and the undoped (reduced, neutral) state of the PPy, respectively. $PPy^{+}(A^{-})$ indicates that the anion A^{-} is incorporated in the polymer as a dopant.

* Corresponding author.
E-mail address: m.rohwerder@mpie.de (M. Rohwerder).

https://doi.org/10.1016/j.corsci.2021.109661
Received 26 March 2021; Received in revised form 28 June 2021; Accepted 1 July 2021
Available online 5 July 2021
0010-938X/© 2021 The Authors. Published by Elsevier Ltd. This is an open access article under the CC BY license (http://creativecommons.org/licenses/by/4.0/).

$PPy^{o} + A^{-}$ indicate that the A^{-} has been expelled into the electrolyte. And C^{+} represents the cation in the electrolyte and it is incorporated into or expelled from the PPy^{o} depending on the size of counterions of A^{-}.

This coupling of electron transfer and the exchange of counterions in the process of electrochemical oxidation and reduction is maybe one of the most interesting aspects of ICPs. Transport of ions has been studied in polymer electrolytes such as Nafion and ICPs using conductivity or diffusion measurements [15]. These studies focus on examining the electrochemical switching of ICP membranes by application of an electric field for the separations of ionic species. Murray et al. have been pioneers to report that PPy deposited on a gold minigrid allows to separate two different solutions, by a potential induced change of the redox states of the PPy which affects the mobility of the ions [16,17]. The results showed a permselectivity for ions can be achieved resulting in ion gate membrane transfer. Also, Ehrenbeck et al. [18] studied the permselectivity of PPy as a function of the oxidation state. They found that incorporation of immobile anions such as dodecylsulfate or n-sulfopropyl-pyrrole leads to modified membranes which exhibit distinct cation permselectivity in the reduced state. Wallace et al. [19,20] worked extensively on electrochemically controlled transport of ionic species across ICP membranes. They reported that the transport of ion species across ICP films can be switched on and off by means of application of an appropriate electrical potential. Also, by the application of different electrical potential waveforms control of the rate of transport and the selectivity of the membrane can be achieved. They emphasized that the exact parameters of the synthesis of the ICPs, especially using different counterions, show a significant influence besides on the general physical and chemical properties especially on the transport properties. Although the correlation between structure of the ICPs and their ionic transport properties is still being developed, there is a wealth of knowledge on factors that influence ionic mobility in ICPs. These studies give a solid proof that ions can be well transport across ICPs and that there is a selectivity for how well ions may move across the ICP matrix. Hence, ICPs are not like conventional non-conducting polymers which act just as barriers for ions, but they provide a means to control the transport of ions.

Concerning redox transitions, usually there will be a mixture of the processes according to Eqs. (1) and (2). But especially, if redox transitions are proliferating over larger distances within ICPs, then this usually results with increased progress of the transition in a preferentially cation exchange-based process, turning the (partially) reduced ICP matrix into a fast cation transport membrane [21]. This makes continuous ICP coatings unsuitable for a triggered release of the counter-anions stored within by corrosion induced ICP reduction, because of the anion release rather cations are incorporated instead [21].

This is also the reason for why although continuous ICP coatings have a certain capability to inhibit corrosion in small pinhole sized defects in the coating, especially in the immersed case, in the presence of a large defect or in the case of a non-immersed sample, where just the defect site is covered by electrolyte, they are observed to disastrously fail [21–26]. However, capsules made of ICPs, incorporated into a matrix of non-conducting polymer, for storing self-healing agents, i.e. corrosion inhibitors or monomers and catalysts for the formation of a new organic coating at the defect, were recently shown to be very promising for realizing smart self-healing coatings which show high performance in terms of safe storage and triggered release [8,9]. The transport of the released active agents, however, was found to be still relatively limited.

Surprisingly the transport of self-healing agents from the coating into the corroding defect site and how it can be optimized are not objects of much research. Most of the current research work on self-healing coatings just focuses on the synthesis of new capsules which are responsive to suitable trigger mechanisms. But only if the released corrosion inhibitor effectively reaches the defect, sufficient self-healing will occur at the defect. Hence, the study of the transport of ions and also of neutral molecules from within the coating to the defect is of crucial importance for the development of high-performing self-healing coatings for corrosion protection [8,27–33].

As mentioned, based on previous work [7] it is clear that continuous ICP coatings can improve signal spreading and thus quickly activate a high number of capsules, leading to effective release of large quantities of active agents. A significantly enhanced transport of released active agents into the defective site(s) would constitute a major step for designing improved self-healing coatings. For these first studies PPy was chosen for the conducting polymer layer and poly(vinyl butyral-co-vinyl alcohol-co- vinyl acetate) (PVB) as non-conducting top-coat. In view of the fact that in many applications, as for instance in the automotive industry, steel is usually used as galvanized steel, Zn was chosen as metallic substrate. A dedicated model sample geometry was used that consisted of a defect in the coating through the PVB and the PPy layer down to the Zn, separated by several millimeters from a reservoir containing corrosion inhibitor ions (see Fig. 1 in Section 2.3). In this set-up, ions and also neutral molecules are able to enter and exit the coating only at the edges, i.e. at the interface with electrolyte at the defect site or at the reservoir. This work is an effort for developing a better understanding of the role of ions transport on self-healing properties and corrosion protection that can be achieved by using redox-active ICPs.

2. Experimental

2.1. Materials

Zn plates (thickness 1.5 mm, 99.95 %) were purchased from Goodfellow and cut into pieces of 15 mm × 20 mm. Potassium chloride (KCl, purity 99 %), hydrogen peroxide (H_2O_2, 30 wt% in H_2O), β-Cyclodextrine (β-CD, purity 97 %), sulfuric acid (H_2SO_4, 98 %), sodium hydroxide (NaOH, reagent grade 98 %), 8-Hydroxyquinoline (8-HQ, purity 99 %), cerium(IV) sulfate ($Ce(SO_4)_2$, reagent type), sodium molybdate (Na_2MoO_4, purity 99.9 %), cerium(III) nitrate hexahydrate ($Ce(NO_3)_3{\cdot}6H_2O$, 99.99 % trace metals basis), pyrrole (reagent grade, 98 %), potassium hydroxide (KOH, ACS reagent, ≥85 %), 3-nitrosalicylic acid (3-Nisa, purity 99 %), ethanol and poly(vinyl butyral-co-vinyl alcohol-co-vinyl acetate) (PVB) (molar mass 50000−80000 g/mol) were supplied by Sigma-Aldrich (Steinheim, Germany). Microscope glass slides were purchase from Hirschmann Laborgeräte GmbH & Co. KG. Pyrrole was purified by distillation under N_2 atmosphere. All other chemicals were used as received unless otherwise noted. All aqueous electrolytes were prepared using water from a USF ELGA water purification system with a conductivity of less than 0.055 μS/cm.

2.2. Electrodeposition of PPy on Zn and Au substrate

Zn plates were ground with P2500 SiC paper (grinding direction parallel to short edge of the specimen), cleaned with water and ethanol, and dried under a nitrogen stream. Before electrodeposition of PPy, the Zn plates were pretreated in a three electrodes set-up by cycling 5 times from −1.1 V to −1.4 V vs Ag/AgCl(3 M KCl) in NaOH (0.25 M) with a scan rate of 10 mV/s using a Voltalab 50 potentiostat. This results in the formation of a protective oxide layer that was found necessary for obtaining a homogeneous and strongly adherent PPy layer in the PPy electrodeposition step [7,34]. The electrodeposition of PPy was realized galvanostatically with a current density of 5 mA/cm^2 in a three-electrode setup, with an area of 8 × 18 mm being exposed to the electrolyte solution consisting of 0.3 M pyrrole and 0.01 M 3-Nisa (pH = 2.5, adjusted with KOH). The thus obtained coatings were washed thoroughly with distilled water and ethanol to remove any excess of monomers. The thickness of the PPy films was about 1.2 μm, controlled at a total passed charge (1.44 C/cm^2).

For quantification of the inhibitor transport, Au evaporated on glass was used as substrate instead of Zn. Prior to the electrodeposition of PPy, the microscope glass slides were pretreated in Piranha solution (with a volume ratio of H_2SO_4 and H_2O_2 of 3:1) to remove the contamination

and organic residues from the glass slides. Onto the thus cleaned glass slides Au layers of 150 nm thickness were deposited by Physical Vapor Deposition (PVD) on the microscope glass slides with a titanium interlayer of 10 nm (also by PVD). PPy was electrodeposited on the Au-coated glass (8 × 18 mm) with a passed charge of 0.313 C/cm^2 for all samples, with a current density 5 mA/cm^2 [7,34]. After the electrodeposition of the PPy on the Zn plates or Au substrate, these samples were spin-coated 4 times with a 5 wt% PVB solution and then further spin-coated 3 times with a 10 wt% PVB solution at 2000 rpm for 20 s, dried in an oven at 75 °C for approx. 10 min, respectively. Also, Zn plates without PPy layer were spin-coated with PVB as reference samples. The samples are denoted in the following as PVB|Zn, PVB|PPy|Zn and PVB|PPy|Au, respectively.

2.3. The experimental model set-up for the ion transport

For the fundamental investigation of the ionic transport to the defect site, a model sample with a separate source reservoir containing the ions of interest was prepared. This reservoir was formed by the PVB|PPy|Zn sample bonded to a piece of glass by using an epoxide paste [35,36]. The edges of glass plates were surrounded by epoxy paste to form the reservoir. A schematic drawing of the experimental set-up for measuring the self-healing performance of ions transports illustrated in Fig. 1, also indicating the measurement of the corrosion potential in the defect and the delamination by SKP.

For the quantification of the corrosion inhibitor transport, a modified set-up as described in Fig. 2 was used, in two variants.

Variant 1: To quantify the ion transport through the (partially) reduced PPy, a PVB|PPy|Zn sample was placed between two reservoirs, one, denoted here as source reservoir, was filled with an aqueous solution containing the corrosion inhibitor (100 µl) to be investigated and the other, denoted here as receiver reservoir, was filled with aqueous 1 M KCl electrolyte (100 µl), respectively. Here the Zn edge exposed to the chloride containing electrolyte corrodes, which causes delamination of the coating. The small Zn area at the Zn edge reduces consumption of inhibitor reaching the reservoir, facilitating its quantification by analysis of the electrolyte. The concentration of the inhibitor ions in the receiver reservoir was then measured by analyzing a well-defined volume of electrolyte taken from the receiver reservoir at given intervals (30 h).

Variant 2: In order to avoid the depletion of the corrosion inhibitor due also to reacting with the Zn surface at the PPy|Zn interface, i.e. to study the true transport through the PPy, also PVB|PPy|Au samples with altogether three reservoirs were used.

One edge of the PPy was in contact with Zn covered by aqueous 1 M KCl (100 µl) solution (with the Zn exposed to the electrolyte serving as anodic defect to drive cathodic delamination, which would not occur for a defect down to Au), the other edge with inhibitor aqueous solution (100 µl) applied on glass as source reservoir (filled with corrosion inhibitor solution, which also inhibits delamination from that side). An artificial defect, serving for collecting the transported inhibitors in a small volume of electrolyte, was inflicted between the two reservoirs and covered with 40 µL 1 M KCl. After 30 h, the electrolyte covering the defect was collected in order to determine the concentration of corrosion inhibitor accumulated there.

For both variants, the distance of source reservoir to the receiver reservoir (variant 1) or defect site (for variant 2: receiver reservoir) was 4.5 mm and the cathodic delamination was in both cases monitored over a distance of 1.5 mm. The concentrations of 3-Nisa, 8-HQ, β-CD, Ce$(SO_4)_2$ and Na_2MoO_4 were 0.015, 0.003, 0.01, 1.0 and 0.2 M in aqueous solution, which is close to the according solubility limit, respectively. The concentration used for the investigations with $Ce(NO_3)_3{\cdot}6H_2O$ were 0.001, 0.05 and 4.0 M.

2.4. Characterization

Scanning Kelvin Probe (SKP)—To investigate the self-healing performance and the cathodic delamination progress an artificial defect (2.5 mm ± 0.2 mm long, 30.5 µm ± 5.4 µm wide, and 42.5 µm ± 6 µm deep) was applied to the coating with a razor blade (see also Fig. 1). The scratch was covered with 7.5 µL 1 M KCl and the sample was subsequently introduced into the SKP chamber with a relative humidity of 93 %. The progress of cathodic delamination at the coating interface and the electrode potential at the defect site were monitored in-situ alternatingly with a commercial SKP system. The SKP tip was calibrated against a Cu/$CuSO_4$ (saturated) reference electrode in air and all potentials are referred to standard hydrogen electrode (SHE) [35,36]. It should be noted, that the PVB|PPy coating cannot stop the progress of cathodic delamination and typically 1.5 mm of the coating was delaminated within just 3 h.

For the progress of the delamination from the defect to the source reservoir the delamination profiles obtained for the PVB|Zn and PVB|PPy|Zn model samples were all quite similar, respectively, regardless of the inhibitors investigated. This is because in that initial stage the situation was always the same: the PVB and PPy were always prepared in the same way and delamination and reduction of the PPy occurred via migration of the same kind of cation (potassium). Only upon onset of inhibition caused by the different inhibitors transported to the defect different behaviour was observed. Here the most notable difference was the increase in corrosion potential. So, just a few typical initial cathodic delamination profiles with different corrosion inhibitors in the source reservoir are presented in the following.

X-ray photoelectron spectroscopy (XPS)—A commercial XPS system (ESCA Quantum 2000 Microprobe) from PHI was used for analyzing the

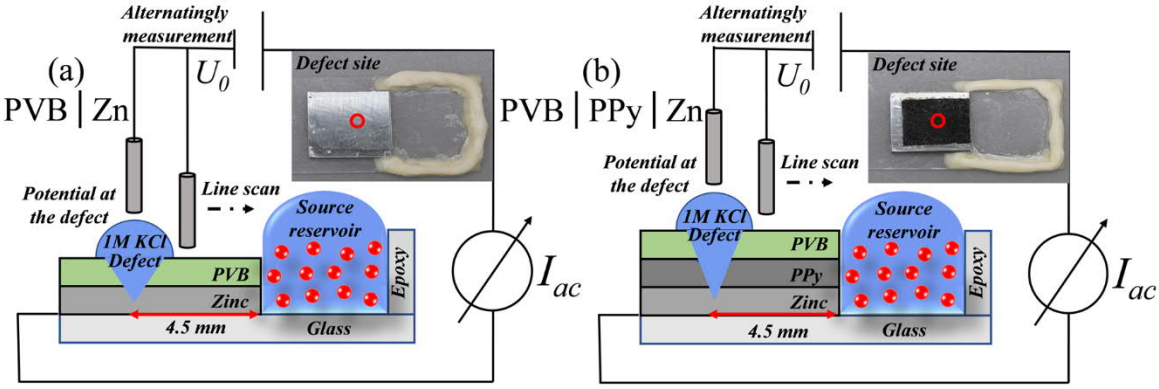

Fig. 1. Experimental setup for measuring the transport efficiency of the coating for ionic or neutral inhibitor molecules via SKP (not to scale). The inserted figures show photos of the set-ups (the red circles represent the position of defect, i.e. a scratch down to the metal covered by a drop of electrolyte). (a) the PVB|Zn model sample; (b) the PVB|PPy|Zn model sample. (For interpretation of the references to colour in this figure legend, the reader is referred to the web version of this article).

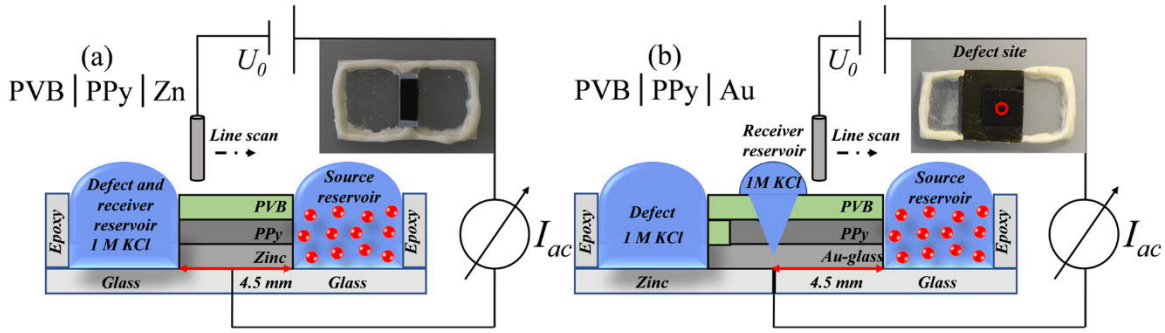

Fig. 2. Experimental setups for quantifying the transport of ionic or neutral inhibitor molecules (not to scale). The inserted figures show photos of the set-ups (again the red circle represents the position of defect). (a) the PVB|PPy|Zn model sample (variant 1); (b) the PVB|PPy|Au model sample (variant 2). (For interpretation of the references to colour in this figure legend, the reader is referred to the web version of this article).

Zn surface at the PPy|Zn interface after pulling off the coating and at the defect site after removal of the electrolyte. The main interest here was on the latter. The received XPS data were all processed and analyzed with CASA XPS. For the PVB|PPy|Zn model samples with Ce^{3+} and Ce^{4+} in the source reservoir, the main focus was on the role of the different oxidation states of the cerium ions for transport and defect passivation. After the experiment on ion transport to the defect site, the PVB|PPy coating was peeled from the Zn substrate and then the defect site was measured with XPS to detect Ce. Note, after the delamination (de-adhesion), the coating could be easily removed from the Zn substrate to expose the bare substrate. The reason for pulling off the coating was to get better access to the Zn surface at the defect.

Inductively coupled plasma mass spectrometry (ICP-MS, NexION 300X, PerkinElmer) and Inductively coupled plasma Optical Emission Spectroscopy (ICP-OES, Iris Intrepid Duo HR) was used to analyze the electrolyte and thus to quantify the amount of Ce^{3+} and Na^{+} which was transported from the source reservoir to the small defect (variant 2) or the receiver reservoir (variant 1) after 30 h, respectively.

3. Results and discussion

In the case of an ICP layer applied onto the metal substrate for enhanced signal spreading [7], the according trigger signal is the corrosion induced decrease of potential. Besides the reduction of the ICP also deadhesion at the ICP|metal interface caused by cathodic delamination needs to be considered, see e.g. [21]. Also at least a partial degradation at the PVB|PPy interface is thinkable [26], although no indications for a delamination at that interface were found. Hence, there are potentially three pathways for the transport of active agents: (i) the (partially) reduced ICP layer, which gets more hydrophilic by its reduction and hence is expected to thus allows a much higher mobility of species than in the initial state, especially for cations [19,20], (ii) along the possibly (partially) delaminated PVB|PPy interface and (iii) along the (partially) delaminated PPy|Zn interface [7,25]. Concerning (ii) and (iii), it is, of course, important that the delaminated interface is also self-healed upon inhibition of the defect. That this indeed can occur was observed in earlier work [7]. Based on the results found here, the most important pathway for the mass transport of inhibitor to the defect is through the (partially) reduced PPy. The specific pathways are indicated in Fig. 3. Note that the reduced PPy has only a low ionic resistivity and hence the iR drop is low, once the delamination/reduction front has passed. Thus, no electric field will oppose the movement of cations from the source reservoir to the defect, ions can hence move in both directions.

This is different from the common observation that during cathodic delamination no anions migrate or diffuse from the defect to the delamination front or cations in the other direction [35,36]. However, this is only due to the electric field along the interface, which drives cations and hinders anions. This field is related to the polarity of the

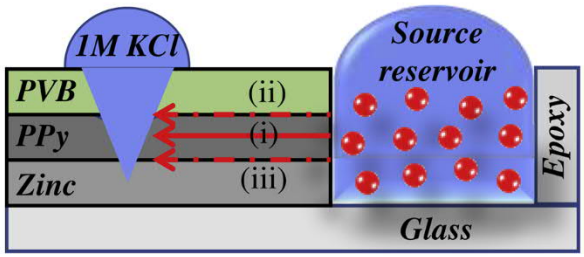

Fig. 3. The corrosion inhibitor species possible transport pathway from the source reservoir to the defect site.

corrosion cell, but the main issue is just the magnitude of that electric field. For the case of Zn as metallic substrate, this corrosion cell will not remain with the delaminated interface as net cathode, as Zn at the interface will to some extent start to corrode. However, reduced PPy provides a quite low ionic resistance. Hence, the Ohmic iR drop is negligible in the delaminated/reduced region. This is crucial for a transport for cations from the source reservoir to the defect. During the delamination process the initial iR drop drives cations from the defect to the delamination front and inhibits anion migration in the same direction. The iR drop would also inhibit cation migration into the other direction to the defect. But the finally negligible iR drop allows ionic migration/diffusion in all directions. Since Zn may also corrode in the delaminated area (unlike it would be the case for iron), the polarity of the corrosion cell might not exist anymore. But regardless of this, the important point here is the absence of an electric field between defect and the delaminated area. So, in this case, both cationic and anionic species can migrate/diffuse in both directions.

3.1. Ion transport along the PVB|Zn interface

Since it seems quite likely that the delaminated interface could play an important role for transporting active agents to the defect, this needed to be investigated first. Fig. 4(a) shows the typical cathodic delamination behavior, monitored by SKP, of a PVB coating applied directly on the surface of Zn. The potential difference between the localized corrosion potential of electrolyte covered defect (actively corroding Zn, typically -0.7 to -0.8 V vs. SHE) and the potential of the intact PVB|Zn interface (passive Zn, typically more anodic potentials near -0.4 V vs. SHE) is the driving force for the cathodic delamination [37]. Where the interface is delaminated, the potential is pulled towards the one of the actively corroding defects. Thus, between the delaminated zone and the intact interface, a very sharp potential slope indicates the delamination front, which over time further proceeds into the intact coating. As can be seen from Fig. 4(a), the delamination of the PVB|Zn model coating proceeds with a rate of about 850 µm/h and the delamination front reaches the reservoir within 3 h. The same behavior was

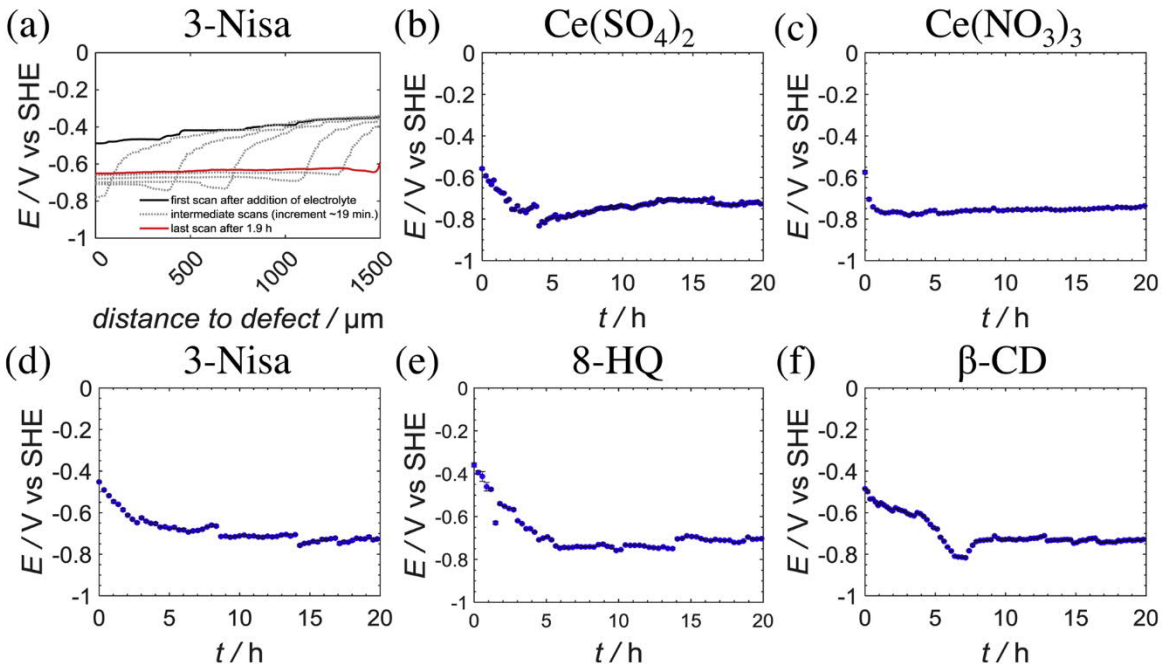

Fig. 4. Results obtained with the PVB|Zn model set-up (see Fig. 1(a)). a) A typically cathodic delamination potential profile between source reservoir and the defect site was recorded by SKP. b-f) The electrode potential was monitored at the defect site for different corrosion inhibitors. The respective concentration of each corrosion inhibitor was the maximum concentration possible, i.e. the concentrations of 3-Nisa, 8-HQ, β-CD, $Ce(SO_4)_2$ and $Ce(SO_3)_3$ were 0.015, 0.003, 0.01, 1.0 and 4.0 M in aqueous solution, respectively.

observed for an experiment where the source reservoir was filled with just distilled water. Also, with the other inhibitors in the source reservoir this initial delamination behavior was the same, as it is just determined by the PVB|Zn interface.

Fig. 4(b–f) show the corrosion potential in the defect site for experiments with different kinds of corrosion inhibitors in the source reservoir. The idea behind these experiments is to find out whether once the delamination front reaches the source reservoir, the delaminated interface may contribute to sufficiently high transport of corrosion inhibitor towards the defective site in order to lead to any significant passivation of the Zn. This should be visible for the here investigated inhibitors, from which Ce^{4+} and the organic inhibitors are quite efficient inhibitors on Zn, as will be shown further below, in form of a significant increase in corrosion potential.

However, in all cases investigated here the electrode potential suggests unchanged ongoing active corrosion of Zn, as indicated by the potential range of -0.7 to -0.8 V vs. SHE over a time of 20 h, which is much larger than the about 3 h necessary to delaminate the coating between the defect and the reservoir containing corrosion inhibitor. All curves show an initial period in which the surface in the defect is increasingly activated, which is indicated by a steady decrease of the corrosion potential until a steady-state value is reached. In none of the cases investigated here an increase from this active corrosion potential can be observed, even after 20 h, i.e. the corrosion inhibitors do not reach the defect site in sufficient amounts as to promote an anodic potential shift towards more positive value characteristic for defect passivation.

These findings fit well with the observation made by Williams and McMurray et al. [38] that during cathodic delamination Ce^{3+} could not enter the delaminating PVB coating|zinc interface from the Ce^{3+} containing aqueous electrolyte in the defect. Although the delamination process provides a driving force for cations from the defect site to migrate into the delaminated interface, the high pH prevailing at the delaminated interface caused its instantaneous precipitation at the border between defect and delaminated interface $Ce(OH)_3$. The formed $Ce(OH)_3$, however, caused the electrode potential in the defect to shift to higher potentials, just as it was expected here, however, did not occur yet.

These results proved that neither the conventional organic coating investigated here, PVB, nor the delaminated interface can serve as efficient ionic transport media over such large distance as investigated here.

3.2. *Lateral ion transport investigated for the PVB|PPy|Zn samples*

3.2.1. *Anionic corrosion inhibitors*

In the following the focus is on the ion transport properties of the (partially) reduced PPy. At first transport of anionic corrosion inhibitors shall be discussed. One anionic corrosion inhibitor chosen for this study was molybdate. Molybdate (VI) is an efficient anionic corrosion inhibitor that works well on Zn, see e.g. [39], where Na_2MoO_4 containing electrolyte in alkaline solution was observed to effectively decrease Zn dissolution. If the MoO_4^{2-} could transport in sufficient amounts from the source reservoir to the defect, it should cause an anodic potential shift [39]. The other anionic corrosion inhibitor investigated here was 3-Nisa, which is another very good corrosion inhibitor on Zn [40,41].

The same experimental set-up as described in section 2.3 (see Fig. 1 (b)) was used for these experiments, however, now a thin layer of PPy was applied directly onto the Zn surface and then a PVB coating was applied on top. Fig. 5(a) shows the potential profiles providing information about the propagation of the delamination front as a function of time. Also, here very well-defined and homogenous delamination curves are observed, with a reduction and delamination rate of about 800 µm/h. Due to the presence of the PPy layer the potential of the intact interface is now much higher than for the PVB|Zn interface, in the range of 0.2 to 0.4 V vs. SHE, and the delaminated zone is between -0.4 to -0.6 V vs. SHE. As explained above for the case when a continuous PPy layer is applied, both PPy reduction and delamination occur and are proceeding simultaneously [21]. Obviously, the corrosion inhibitor in the source reservoir has no effect on the reduction/delamination process at the interface.

Most importantly, also no or only little effect on the corrosion potential in the defect is observed for both kinds of anionic corrosion

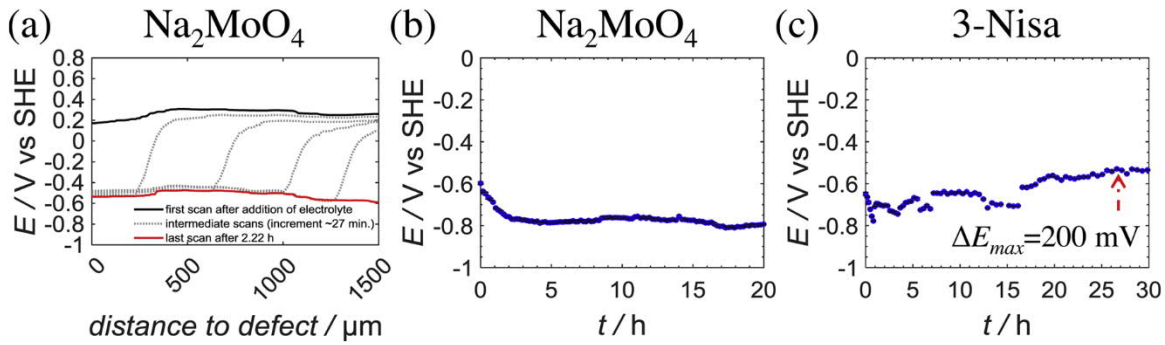

Fig. 5. Results obtained with the PVB|PPy|Zn model set-up (see Fig. 1(b)). a) A typically representative figure of the cathodic delamination potential profiles. b-c) Electrode potential was monitored by SKP at the defect site with different corrosion inhibitors. The respective concentration of each corrosion inhibitor was the respective maximum concentration possible, i.e. the concentrations of 3-Nisa and Na_2MoO_4 were 0.015 and 0.2 M in aqueous solution, respectively.

inhibitor in the source reservoir (see Fig. 5(b) and (c)), as the potentials remain at the typical low values characteristic for active corrosion of Zn. This means that no sufficient transport of anionic corrosion inhibitor occurred from the source reservoir to the defect. This is interesting in view of the fact that in an earlier works, for both PVB|Zn [8] as well as PVB|PPy|Zn [7], it was observed that e.g. 3-Nisa released from polyaniline (PANI) capsules could reach the defect in sufficient amount in order to lead to its passivation. However, in these cases the released anionic corrosion inhibitor molecules did not have to diffuse over several millimeters, as is the case in this experiment. Instead in these cases the capsules containing the anionic corrosion inhibitor were distributed in relatively high density at the interface. Hence, it can be assumed that the main part of corrosion inhibitor reaching the defect will originate from capsules relatively close to the defect. Here, however, all corrosion inhibitor reaching the defect has to overcome the several millimeters distance separating defect and source reservoir. In fact, that is the intention of these experiments, to evaluate how the transport of active agents can be improved.

Previous studies have demonstrated the insertion of cations into and release of ions from PPy coating during it reduction depend on the size of the ions in the electrolyte and of the counterions in the PPy coating [19, 20]. If the counterions are small enough, they are released from the PPy coating to into the electrolyte solution during the reduction for charge compensation. In the case of large counterions, the charge compensation takes place preferentially by cation insertion. In most cases, a mixed anion release/cation incorporation process is observed depending on the size of the counterions and the cations in the electrolyte solution. However, if the reduction has to proceed over extended distances, such as for the case of reduction spreading laterally from a defective site into a PPy layer, then even for ICP coatings with relatively small counter-anions the overall reduction process will be mainly supported by charge neutralization via cation incorporation, because anions remaining in the matrix increasingly turn the matrix cation permselective, leading to a high mobility for cations and a low one for anions [21]. This is in accordance with work showing that from a PPy(3-Nisa) coating the 3-Nisa cannot be released or just to a small amount, and instead cations from the defect were incorporated during the reduction process [25]. This cation permselectivity could be the reason why anionic corrosion inhibitors do not reach the defect in high enough quantity as to lead to significant passivation. However, it should be pointed out that for 3-Nisa in the source reservoir still a small shift towards higher potentials by about 200 mV can be observed. Moreover, the potential is not even reaching the low values characteristic for full activation of the corrosion. This indicates that different from the case without the PPy layer some amount of 3-Nisa has reached the defect before full activation occurred, inhibiting full activation. But the effect is much weaker than in the mentioned previous work where release of 3-Nisa occurred from PANI capsules distributed at high density at the interface [7,8].

3.2.2. *Cationic corrosion inhibitors*

For the investigation of cationic transport besides monitoring the corrosion potential in the defect also a quantification of the amount of inhibitor reaching the defect from the source reservoir was carried out. A special PVB|PPy|Au sample set-up (variant 2, see Fig. 2(b)) was designed for these experiments targeted at providing quantified information of achieved concentrations of corrosion inhibitor having reached from the source reservoir to the defect. The advantage of this set-up avoids the depletion of corrosion inhibitor on the Zn surface at the delaminated interface during the transport process and thus allows obtaining more reliable data about the principal transport properties of especially the PPy layer for corrosion inhibitor. After 30 h, the solution of transported corrosion inhibitor was collected and measured by ICP-MS(OES). For comparison also experiments with a variant 1 set-up (see Fig. 2(a)) were carried out, i.e. with a PVB|PPy|Zn configuration.

The partial reduction/delamination of the PPy layer in the PVB|PPy|Au sample (Variant 2) set-up was monitored by SKP and a typical example is shown in Fig. 6(a). The progress of the delamination is clearly visible and its rate was about 750 µm/h. The result shows that the potential of intact interface is between 0.2 and 0.4 V vs. SHE and the potential at the reduced/delaminated area is in the range between -0.4 and -0.6 V vs. SHE. The progress of the delamination front was recorded by SKP and the delamination was found to proceed with a homogeneous rate, similar as the cases discussed above. Ce^{3+} as a well-known corrosion inhibitor has been widely investigated for application in aqueous environment [42–45]. The inhibition mechanism of Ce^{3+} is based on interacting with OH^- to form hydroxide precipitates, thus relying partly on the cathodic oxygen reduction reaction to form OH^- and to cause a local pH increase at cathodic sites. Here, Ce^{3+} was chosen as cationic corrosion inhibitor to study the ionic transport of cationic corrosion inhibitor from the source reservoir to the defect and whether that will be sufficient to significantly passivate the defect site.

Fig. 6(b) shows the accumulative concentration of Ce^{3+} having reached the defect after diffusing from the source reservoir laterally across the PVB|PPy|Zn sample (Variant 1, see Fig. 2(a)) once the reduction/delamination has reached the receiver reservoir, as measured by ICP-MS. The delamination behavior in this case is again as shown in Fig. 5(a). In this series of experiments, the initial Ce^{3+} concentrations in the source reservoirs were adjusted to 0.001, 0.05 and 4.0 M, respectively. After 30 h of duration of these transport experiments, the Ce^{3+} concentration in the receiver reservoir (Variant 1) were 8, 11 and 288 nM, respectively. These results indicate a very limited successful Ce^{3+} transport through the delaminated zone to reach the receiver reservoir (Variant 1). Although there does not seem to be a simple correlation between the concentration of Ce^{3+} in the source reservoir and the one found in the receiver reservoir (Variant 1), it is obvious that the highest concentration in the source reservoir also resulted in a corresponding higher concentration in the receiver reservoir (Variant 1).

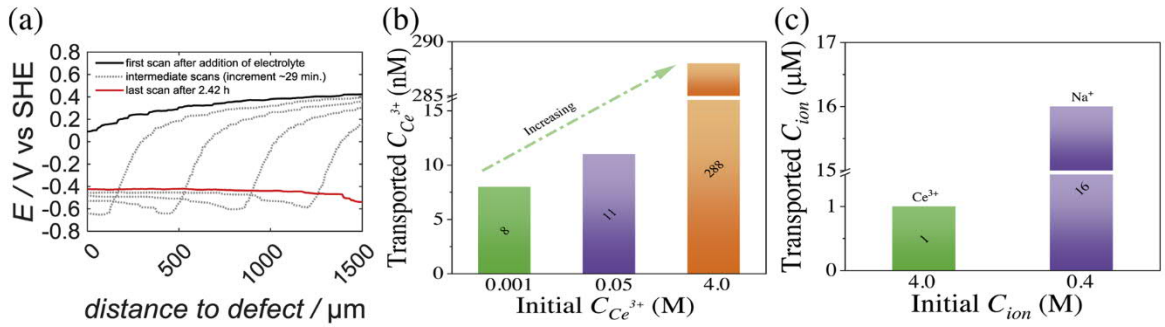

Fig. 6. a) Example for a typical delamination profile for PVB|PPy|Au sample (here with Na_2MoO_4 aqueous in source reservoir, Variant 2, see Fig. 2(b)). b) Cumulative transport of Ce^{3+} from the source reservoir to the receiver reservoir in the PVB|PPy|Zn sample set-up (Variant 1, see Fig. 2(a)). The concentrations of $Ce(NO_3)_3$ in the source reservoirs were 0.001, 0.05, and 4.0 M, respectively. c) Cumulative concentration of Na^+ and Ce^{3+} from the source reservoir to the defective site in the PVB|PPy|Au sample set-up (Variant 2, see Fig. 2(b)). The concentrations of Ce^{3+} and Na^+ were 4.0 and 0.4 M, respectively.

The results clearly indicate that Ce^{3+} can move through the (partially) reduced PPy layer, but not at a significant rate.

Of course, it is expected that transfer from the source reservoir to the defect across the reduced PPy will depend especially on charge of the ions and ionic radii. For more complex species also, interaction of certain functional groups with the reduced PPy matrix might play a role.

Although, no detailed study was carried out yet on the question of relative transfer numbers for different kind of ions, a direct comparison between Ce^{3+} and Na^+ shows that huge differences can be expected. Although the maximum concentration of Na^+ (owing to the solubility of the Na_2MoO_4, as in the source reservoir always corrosion inhibitor has to be used, in order to prevent delamination also from that side) was only about a tenth of the one investigated for Ce^{3+}, the amount of Na^+ found accumulated after 30 h in the defect sites was about eight times higher (see Fig. 6(c), Variant 2). Although the volume of the electrolyte in the receiver reservoir is different (see in Section 2.3, Variant 1 and Variant 2), it should be also noted that here indeed the Ce^{3+} concentration is significantly higher than in the experiments carried out with variant 1 (see Fig. 6(b)), which might be due to less consumption on the Au surface compared to the Zn surface during transport at the PPy|metal interface.

Nevertheless, for the higher Ce^{3+} concentrations in the source reservoir Ce^{3+} enrichments in the receiver reservoir were found to reach levels that are already relevant for many corrosion inhibitors. Hence, also experiments were carried out with a focus on the effect on the corrosion potential, using the PVB|PPy|Zn model set-up (see Fig. 1(b)) and monitoring the corrosion potential by SKP.

Fig. 7(a–d) shows the evolution of the potential in the defect for the cases of Ce^{3+} and for Ce^{4+} as a function of time for PVB|PPy|Zn model set-up (see Fig. 1 (b)). For Ce^{3+} in the source reservoir, the potential at the defect just stays at the potential of active corrosion of Zn, whatever the concentration of Ce^{3+} in the source reservoir. After the experiments with Ce^{3+}, the reduced/delaminated PVB|PPy coatings were peeled off from the Zn surface, which was positioned left from the source reservoir (see description in the Section 2.4) and XPS analysis of the surface of the former Zn defect was carried out. No Ce^{3+} was found on the surface in the defect (see red curve in Fig. 7(e)). Obviously, no $Ce(OH)_3$ precipitation occurred in the defect. This looks like that the Ce^{3+} transportation results (Fig. 6(b)) measured by ICP-MS disagree with these results obtained by XPS. As we mentioned before, when using the PVB|PPy|Zn model coatings connected with two reservoirs (Variant 1, see Fig. 2(a)) it was possible to detect the Ce^{3+} in the receiver reservoir although the concentration was quite low. Due to this very limited amount of Ce^{3+}, the Zn at the defect is not passivated. That means that the low amounts of Ce^{3+} having reached there will be diluted in the volume of corrosion products that are forming uninhibited. Hence, the concentration remained below the detection limit of XPS.

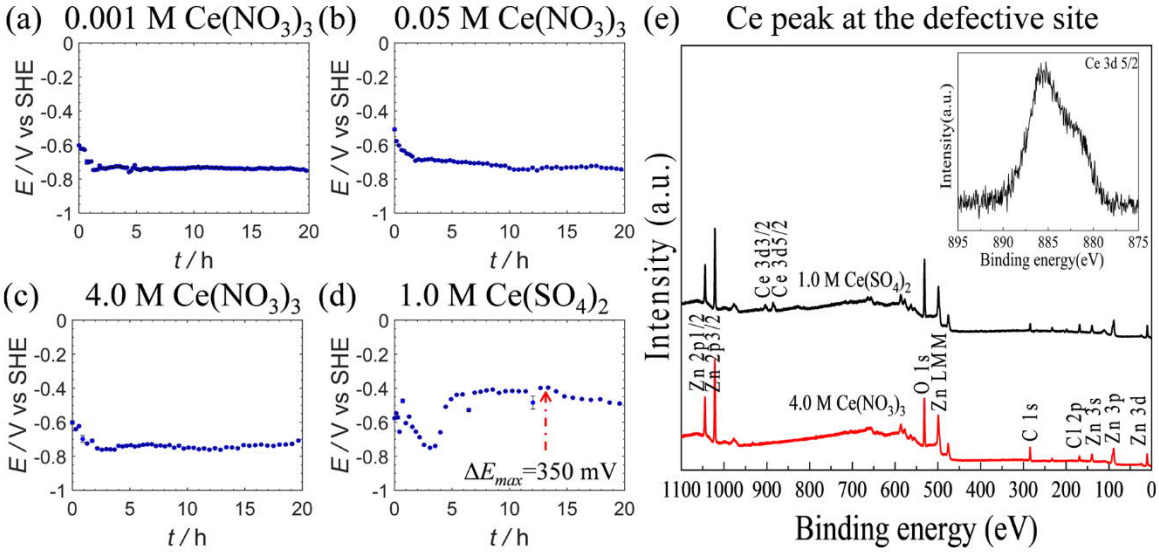

Fig. 7. a–d) Corrosion potential as monitored by SKP at the defect for Ce^{3+} and Ce^{4+} present in the source reservoir. These results were obtained with the PVB|PPy|Zn model set-up (see Fig. 1(b)). Note, the initial concentration of Ce^{3+} in the source reservoirs are 0.001, 0.05, and 4.0 M, for (a), (b) and (c), respectively. The initial concentration of Ce^{4+} is 1.0 M for (d). e) XPS survey spectra obtained on the defect at the indicated concentration in the source reservoir after stopping the experiment and removal of electrolyte and coating. The insert shows a high resolution of the Ce $3d^{5/2}$ peak of the Ce^{4+} in the defect.

One key factor for the low Ce^{3+} transfer to the defect (for example compared to Na^+, see Fig. 6(c)) is proposed to be its likely precipitation during transport by reacting with OH^- that is produced at the delaminated interface and according precipitation of the hydroxide, as at the delaminated interface the pH is quite high, much higher than in the defect (which is well below pH 8) where hence precipitation is not expected [46]. This might be even the main reason why no passivation occurred.

Hence, also Ce^{4+} was investigated as a cationic corrosion inhibitor and its transport was studied with a PVB|PPy|Zn set-up (see Fig. 1(b)) and also the correlated self-healing performance was investigated. Due to the low solubility of Ce^{4+} in aqueous electrolyte, there is up to date only a very limited number of reports on Ce^{4+} as corrosion inhibitor for corrosion protection, and these are limited to strong acid conditions [47–51]. According to the Pourbaix diagram of cerium, Ce^{4+} combines with OH^- to form $Ce(OH)^{3+}$, $Ce(OH)_2^{2+}$ $Ce(OH)_3^+$ when the pH below 4. If the pH further increases, Ce^{4+} will react with OH^- to form stable $Ce(OH)_4$ precipitates [46]. Hence, significant loss of Ce^{4+} is therefore expected during its transport from the source reservoir to the defect, but different from Ce^{3+} at the defect it should readily precipitate as $Ce(OH)_4$.

Fig. 7(d) shows that a huge anodic potential shift of more than 350 mV is observed when Ce^{4+} is put as corrosion inhibitor into the source reservoir. Once the PPy is completely delaminated between the defect and the source reservoir, within 3 h the electrode potential at the defect shows a quick response and increases towards more positive values. After about 5 h the electrode potential does not further change and stays at about −400 mV vs. SHE, which is characteristic for passive Zn. After the experiment, XPS was used to further trace the path of Ce^{4+} and it was found that Ce^{4+} passivated the defect. Indeed, a clearly visible Ce^{4+} peak was found by XPS at the defect, as can be seen in Fig. 7(e) (black curve and insert). Thus, it is proven that Ce^{4+} has a sufficient transportability and can passivate the defect.

This good performance is attributed to the good cation transport properties of the (partially) reduced PPy. This is due to the fact that most of its 3-Nisa doped into it as counter-anions during its electrodeposition is not released during delamination (as discussed above), which leads to high cation mobility [21], leading to still sufficient transport despite high loss by precipitation.

The here observed striking difference in the performance of Ce^{3+} and Ce^{4+} is proposed to be mainly due to the much higher inhibition efficacy of Ce^{4+} at the neutral to slightly alkaline pH levels prevailing in the defect in comparison to Ce^{3+}. Hence, Ce^{4+} shows the better performance although it should suffer considerable loss by precipitation already during transport from the source reservoir within the PPy layer and/or at the PPy|metal interface. Ce^{3+} is present mainly in the form of free Ce^{3+}, and no precipitation occurs in the defect. So, some loss during its transport may be expected, as already mentioned, but only little precipitation at the defect. Only above pH values of 9, the precipitant $Ce(OH)_3$ will form to passivate the defect. However, Ce^{4+} is mainly present in the form of free hydrated Ce^{4+} ions. Precipitation of $Ce(OH)_4$ is already expected to start above pH 2 [46]. It is assumed that the (partially) reduced PPy film with its high cation permselectivity at least partially prevents that, most likely also by a not too high pH, due to some acidity retained from the deposition process and by smearing out oxygen reduction across the layer (see [21] and especially [26]). The Ce^{4+} inhibits the corrosion in the defect by forming cerium metal hydroxide and oxide passive layer over the defect and thereby blocking the cathodic reaction site.

This example shows, that it is not sufficient that inorganic corrosion inhibitors can be transported relatively well. It is of course also important that under the conditions at the defect they lead to effective inhibition of corrosion. However, obviously the (partially) reduced PPy allows for quite efficient transport of cations. As the number of inorganic cationic corrosion inhibitors is not very high, organic corrosion inhibitors, that are expected, however, to be in their uncharged form under the conditions investigated here, were also investigated in this work. The mobility of uncharged inhibitor molecules is expected to be significantly improved in the (partially) reduced PPy by its increased hydrophilicity compared to the (half) oxidized one.

A number of organic compounds have been described as efficient metal corrosion inhibitors. Some of these were chosen to study their transport and passivation performance in our PVB|PPy|Zn model sample set-up (see Fig. 1(b)). β-CD has been widely used in the field of pharmaceutical and biomedical research as a supramolecular host, but recently a few reports were published about using it also as corrosion inhibitor for corrosion protection [52–55]. 8-HQ is a of mixed type corrosion inhibitor that is widely used for corrosion inhibition for Al, Cu and Mg. The inhibitory mechanism has been studied and the results indicate that 8-HQ adsorbs on the metal surface to form a metal-HQ complex chelate which slows down the corrosion rate and blocks aggressive species [56].

Fig. 8(a and b) shows that the anodic potential shift in the defect, upon successful transport from the source reservoir, is more than 600 mV for all two investigated organic corrosion inhibitors, especially for 8-HQ the electrode potential increases more than 700 mV. These results indicate that 8-HQ and β-CD both have a good transportability from the source reservoir to the defect through the (partially) reduced PPy coating. For the electrode potential curves, within the first 10 h just the active corrosion potential of Zn is observed, and then a progressive increase of the electrode potential. Finally, a stable and very high potential value is reached, indicating very efficient passivation of the defect.

Very surprising is the extremely high anodic shift of the corrosion potential as a consequence of passivation. Such high anodic shifts could not be observed in separate studies on the passivation of Zn with these organic corrosion inhibitors. It is hence proposed that the observed strong passivation behavior is due to a synergy between the passivating effect caused by the corrosion inhibitor and an anodization effect caused by the re-oxidized PPy, that in turn is caused by the passivation of the defect and the delaminated interface.

This effect is not only observed for organic inhibitors. For instance, it is well known that 3-Nisa can effectively passivate Zn in aqueous chloride solution [8,40,41]. For composite coatings of PVB and 3-Nisa loaded PANI capsules applied on Zn a significant passivation of a defect inflicted into the coating, caused by corrosion induced smart release, was observed in an earlier work [8]. The anodic potential shift in the defect observed in that work was about 340 mV, as monitored by SKP [8]. This is different when a PPy layer is electrodeposited onto the Zn, with 3-Nisa counter-anions. In that case not enough 3-Nisa release from the PPy(3-Nisa) coating is observed for a passivation of the defect, due to preferred incorporation of cations [7]. For the PVB|PPy|Zn model samples investigated in this work some effect was observed for the transport of the 3-Nisa from the source reservoir to the defect, where the corrosion potential showed an anodic shift by almost 200 mV (Fig. 5(c)), showing that even across this quite significant distance some 3-Nisa can reach the defect and can cause some degree of passivation, but not enough for re-oxidation of the PPy. However, experiments showed that PVB|3-Nisa@PANI|PPy|Zn coatings, where 3-Nisa loaded PANI capsules and PVB were coated onto a PPy layer electrodeposited onto Zn, caused the corrosion potential at the defect site to increase by more than 670 mV [7]. The result showed that a layer of PPy combined with 3-Nisa@PANI capsules, which lead already to a significant 3-Nisa supply to the defect [8], can significantly improve the passivation [7], in a similar way as is now observed here for the two investigated organic inhibitors.

From these observations it is obvious that combining sufficient supply of the corrosion inhibitor with the redox-active PPy can lead to strong synergetic effects. Obviously, the amount of Ce^{4+} that was transported to the defect in the experiments described above was not high enough to enable that synergetic effect (see Fig. 7(d)).

Hence, the good self-healing performance observed for the organic

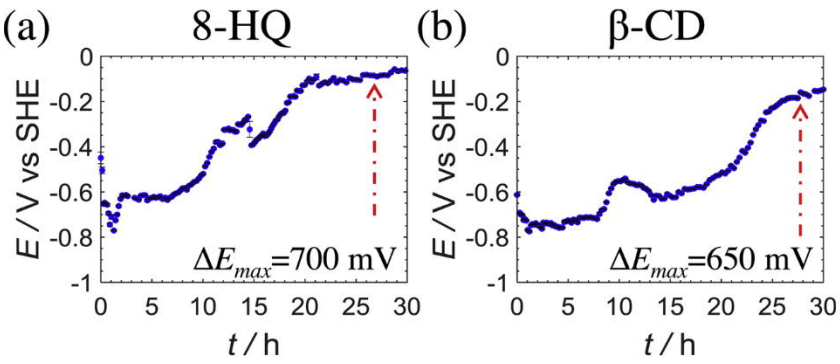

Fig. 8. Results obtained with the PVB|PPy|Zn model set-up (see Fig. 1(b)). a-b) Electrode potential monitored by SKP at the defect with two different organic corrosion inhibitors in the source reservoir. Again, the concentrations were the respective highest soluble concentrations, i.e. the concentrations of 8-HQ and β-CD were 0.003 and 0.01 M in aqueous solution, respectively.

corrosion inhibitors (8-HQ and β-CD) is proposed to be due mainly to sufficient transport, allowing high enough concentrations to accumulate in the defect that are sufficient to directly passivate the Zn which in turn enables the PPy to re-oxidized, which then triggers further anodic polarization. When the organic corrosion inhibitor is used alone or just the PPy coating, such a high inhibition efficiency is not observed.

4. Conclusions

The focus of this work is the lateral ionic transport as an important prerequisite for successful passivation and/or self-healing of defects by smart self-healing coatings. Based on previous works one focus was on the delaminated interface, another on the (partially) reduced conducting polymer (here PPy), applied as a layer directly onto the metal surface. Here, several model set-ups (denoted as PVB|Zn, PVB|PPy|Zn and PVB|PPy|Au) were used to investigate the transport of active agents. A combination of localized corrosion monitoring and chemical analysis was applied to provide comprehensive information about the quantitative ion transport for optimization of intelligent self-healing coating systems. The following conclusions can be made:

1) A layer of (partially) reduced PPy provides superior inhibitor transport to the defect site compared to a delaminated interface.
2) The mobility of cationic corrosion inhibitors through the (partially) reduced PPy seems to be higher than the one of anionic ones, which is proposed to be due to the cation-permselectivity of the (partially) reduced PPy matrix, with quite immobile counter-anions. Also, the transport of (uncharged) organic inhibitors was found to be high in the (partially) reduced PPy, most likely due to its increased hydrophilicity.
3) The (partially) reduced PPy layer even enables transport of species precipitating at already quite low pH.
4) Finally, and unexpectedly it was found that the use of a PPy layer does not only lead to an improved corrosion inhibitor transport to the defective site, but also results in a synergetic improved defect passivation by the combined effect of the corrosion inhibitor and an electrochemically driven passivation through the re-oxidizing PPy, once sufficient corrosion inhibitor has reached the defect. Potential shifts by up to 700 mV were observed, which is much higher than what can be provided by the inhibitors alone.

In summary, a model set-up was used to investigate the transport of corrosion inhibitors along delaminated interfaces and through (partially) reduced PPy. As could be shown, the PPy layer can significantly enhance the corrosion inhibitor transport, which is important to passivate defect and design self-healing coating. It will be useful to study in more detail the relationship of structure vs. ion transport properties in this important class of self-healing coating.

CRediT authorship contribution statement

Yue Yin: Conceptualization, Validation, Investigation, Methodology, Writing - original draft. **Matthias Schulz:** Conceptualization, Methodology, Validation. **Michael Rohwerder:** Supervision, Conceptualization, Validation, Writing - review & editing.

Declaration of Competing Interest

The authors report no declarations of interest.

Acknowledgments

Yue Yin gratefully acknowledges the financial support from China Scholarship Council funding and also the Max-Planck Society for partial funding. We thank Manoj Prabhakar for the XPS, Andrea Mingers for the ICP-MS, Daniel Kurz for the ICP-OES measurements.

References

[1] E. Stavrinidou, P. Leleux, H. Rajaona, D. Khodagholy, J. Rivnay, M. Lindau, S. Sanaur, G.G. Malliaras, Direct measurement of ion mobility in a conducting polymer, Adv. Mater. 25 (2013) 4488–4493.
[2] E. Stavrinidou, M. Sessolo, B. Winther-Jensen, S. Sanaur, G.G. Malliaras, A physical interpretation of impedance at conducting polymer/electrolyte junctions, AIP Adv. 4 (2014), 017127(1-6).
[3] E. Stavrinidou, P. Leleux, H. Rajaona, M. Fiocchi, S. Sanaur, G.G. Malliaras, A simple model for ion injection and transport in conducting polymers, J. Appl. Phys. 113 (2013), 244501(1-6).
[4] M.R. Anderson, B.R. Mattes, H. Reiss, R.B. Kaner, Conjugated polymer films for gas separations, Science 252 (1991) 1412–1415.
[5] L.V. Kayser, D.J. Lipomi, Stretchable conductive polymers and composites based on PEDOT and PEDOT: PSS, Adv. Mater. 31 (2019), 1806133(1-13).
[6] J. Janata, M. Josowicz, Conducting polymers in electronic chemical sensors, Nat. Mater. 2 (2003) 19–24.
[7] M. Uebel, L. Exbrayat, M. Rabe, T.H. Tran, D. Crespy, M. Rohwerder, On the role of trigger signal spreading velocity for efficient self-healing coatings for corrosion protection, J. Electrochem. Soc. 165 (2018) C1017–C1027.
[8] A. Vimalanandan, L.P. Lv, T.H. Tran, K. Landfester, D. Crespy, M. Rohwerder, Redox responsive self-healing for corrosion protection, Adv. Mater. 25 (2013) 6980–6984.
[9] T.H. Tran, A. Vimalanandan, G. Genchev, J. Fickert, K. Landfester, D. Crespy, M. Rohwerder, Regenerative nano-hybrid coating tailored for autonomous corrosion protection, Adv. Mater. 27 (2015) 3825–3830.
[10] K.M. Cheung, D. Bloor, G.C. Stevens, The influence of unusual counterions on the electrochemistry and physical properties of polypyrrole, J. Mater. Sci. 25 (1990) 3814–3837.
[11] J.R. Reynolds, N.S. Sundaresan, M. Pomerantz, S. Basak, C.K. Baker, Self-doped conducting copolymers: a charge and mass transport study of poly{pyrrole-CO[3-(pyrrol-1-YL)propanesulfonate]}, J. Electroanal. Chem. Interfacial Electrochem. 250 (1988) 355–371.
[12] E. Smela, N. Gadegaard, Surprising volume change in PPy(DBS): an atomic force microscopy study, Adv. Mater. 11 (1999) 953–957.
[13] A.C. Partridge, Ion transport membranes based on conducting polymers, Electrochim. Acta 40 (1995) 1199–1202.
[14] X.Z. Wang, E. Smela, Color and volume change in PPy(DBS), J. Phys. Chem. C 113 (2009) 359–368.

[15] R.M. Penner, C.R. Martin, Ion transporting composite membranes I. nafion-impregnated gore-tex, J. Electrochem. Soc. 132 (1985) 514–515.
[16] P. Burgmayer, R.W. Murray, An ion gate membrane: electrochemical control of ion permeability through a membrane with an embedded electrode, J. Am. Chem. Soc. 104 (1982) 6139–6140.
[17] P. Burgmayer, R.W. Murray, Ion gate electrodes. Polypyrrole as a switchable ion conductor membrane, J. Phys. Chem. 88 (1984) 2515–2521.
[18] C. Ehrenbeck, K. Juttner, Ion conductivity and permselectivity measurements of polypyrrole membranes at variable states of oxidation, Electrochim. Acta 41 (1996) 1815–1823.
[19] H. Zhao, W.E. Price, G.G. Wallace, Effect of the counterion employed during synthesis on the properties of polypyrrole membranes, J. Membr. Sci. 87 (1994) 47–56.
[20] A.C. Partridge, C. Milestone, C.O. Too, G.G. Wallace, Ion transport membranes based on conducting polymers, J. Membr. Sci. 132 (1997) 245–253.
[21] M. Rohwerder, A. Michalik, Conducting polymers for corrosion protection: What makes the difference between failure and success? Electrochim. Acta 53 (2007) 1300–1313.
[22] M. Rohwerder, L.M. Duc, A. Michalik, In situ investigation of corrosion localised at the buried interface between metal and conducting polymer based composite coatings, Electrochim. Acta 54 (2009) 6075–6081.
[23] M. Rohwerder, S. Isik-Uppenkamp, C.A. Amarnath, Application of the Kelvin Probe method for screening the interfacial reactivity of conducting polymer based coatings for corrosion protection, Electrochim. Acta 56 (2011) 1889–1893.
[24] G. Paliwoda-Porebska, M. Stratmann, M. Rohwerder, K. Potje-Kamloth, Y. Lu, A. Z. Pich, H.J. Adler, On the development of polypyrrole coatings with self-healing properties for iron corrosion protection, Corros. Sci. 47 (2005) 3216–3233.
[25] G. Paliwoda-Porebska, M. Rohwerder, M. Stratmann, U. Rammelt, L.M. Duc, W. Plieth, Release mechanism of electrodeposited polypyrrole doped with corrosion inhibitor anions, J. Solid-State Electrochem. 10 (2006) 730–736.
[26] A. Michalik, M. Rohwerder, Conducting polymers for corrosion protection: a critical view, Zeitschrift für Physikalische Chemie 219 (2005) 1547–1559.
[27] D.G. Shchukin, M. Zheludkevich, K. Yasakau, S. Lamaka, M.G.S. Ferreira, H. Möhwald, Layer-by-Layer assembled nanocontainers for self-healing corrosion protection, Adv. Mater. 1 (2006) 1672–1678.
[28] Y.M. Lvov, D.G. Shchukin, H. Mohwald, R.R. Price, Halloysite clay nanotubes for controlled release of protective agents, ACS Nano 2 (2008) 814–820.
[29] M.F. Montemor, Functional and smart coatings for corrosion protection: a review of recent advances, Surf. Coat. Technol. 258 (2014) 17–37.
[30] S.A. Haddadi, S.A.A. Ramazani, M. Mahdavian, P. Taheri, J.M.C. Mol, Fabrication and characterization of graphene-based carbon hollow spheres for encapsulation of organic corrosion inhibitors, Chem. Eng. J. 352 (2018) 909–922.
[31] Y. González-García, S.J. García, A.E. Hughes, J.M.C. Mol, A combined redox-competition and negative-feedback SECM study of self-healing anticorrosive coatings, Electrochem. Commun. 13 (2011) 1094–1097.
[32] L.W. Ma, J.K. Wang, D.W. Zhang, Y. Huang, L.Y. Huang, P.J. Wang, H.C. Qian, X. G. Li, H.A. Terryn, J.M.C. Mol, Dual-action self-healing protective coatings with photothermal responsive corrosion inhibitor nanocontainers, Chem. Eng. J. 404 (2021) 127118.
[33] H.C. Qian, D.K. Xu, C.W. Du, D.W. Zhang, X.G. Li, L.Y. Huang, L.P. Deng, Y.C. Tu, J.M.C. Mol, H.A. Terryn, Dual-action smart coatings with a self-healing superhydrophobic surface and anti-corrosion properties, J. Mater. Chem. A 5 (2017) 2355–2364.
[34] M. Uebel, Release and Transport of Corrosion Inhibitors in Self-healing Coatings for Intelligent Corrosion Protection, Ruhr-Universität Bochum, 2019.
[35] A. Leng, H. Streckel, M. Stratmann, The delamination of polymeric coatings from steel. Part1: calibration of the Kelvin probe and basic delamination mechanism, Corros. Sci. 41 (1999) 547–578.
[36] A. Leng, H. Streckel, M. Stratmann, The delamination of polymeric coatings from steel. Part 2: first stage of delamination, effect of type and concentration of cations on delamination, chemical analysis of the interface, Corros. Sci. 41 (1999) 579–597.
[37] R. Hausbrand, M. Stratmann, M. Rohwerder, The physical meaning of electrode potentials at metal surfaces and Polymer/metal interfaces: consequences for delamination, J. Electrochem. Soc. 155 (2008) C369–C379.
[38] G. Williams, H.N. McMurray, D.A. Worsley, Cerium(III) inhibition of corrosion-driven organic coating delamination studied using a scanning kelvin probe technique, J. Electrochem. Soc. 149 (2002) B154–B162.
[39] V. Shkirskiya, P. Keil, H. Hintze-Bruening, F. Leroux, T. Stimpfling, D. Dragoe, K. Ogle, P. Volovitch, MoO_4^{2-} as a soluble inhibitor for Zn in neutral and alkaline solutions, Corros. Sci. 99 (2015) 31–41.
[40] B. Muller, J. Langenbucher, Complete corrosion inhibition of lamellar zinc pigment in aqueous alkaline media, Corros. Sci. 45 (2003) 395–401.
[41] A. Vimalanandan, Investigation of Redox-responsive Coatings for Zinc Corrosion Protection, Ruhr-Universität Bochum, 2015.
[42] S. Kallip, A.C. Bastos, K.A. Yasakau, M.L. Zheludkevich, M.G.S. Ferreira, Synergistic corrosion inhibition on galvanically coupled metallic materials, Electrochem. Commun. 20 (2012) 101–104.
[43] K. Aramaki, The inhibition effects of cation inhibitors on corrosion of zinc in aerated 0.5 M NaCl, Corros. Sci. 43 (2001) 1573–1588.
[44] K. Aramaki, Synergistic inhibition of zinc corrosion in 0.5 M NaCl by combination of cerium(III) chloride and sodium silicate, Corros. Sci. 44 (2002) 871–886.
[45] M.F. Montemor, A.M. Simões, M.G.S. Ferreira, Composition and corrosion behaviour of galvanised steel treated with rare-earth salts: the effect of the cation, Prog. Org. Coat. 44 (2002) 111–120.
[46] B. Bouchaud, J. Balmain, G. Bonnet, F. Pedraza, pH-distribution of cerium species in aqueous systems, J. Rare Earths 30 (2012) 559–562.
[47] X.H. Li, S.D. Deng, H. Fu, G.N. Mu, Synergistic inhibition effect of rare earth cerium (IV) ion and 3,4-dihydroxybenzaldehye on the corrosion of cold rolled steel in H_2SO_4 solution, Corros. Sci. 51 (2009) 2639–2651.
[48] P. Rodic, I. Milosev, Corrosion inhibition of pure aluminium and alloys AA2024-T3 and AA7075-T6 by cerium(III) and cerium(IV) salts, J. Electrochem. Soc. 163 (2016) C85–C93.
[49] D.Q. Zhang, H. Wu, L.X. Gao, Synergistic inhibition effect of l-phenylalanine and rare earth Ce(IV) ion on the corrosion of copper in hydrochloric acid solution, Mater. Chem. Phys. 133 (2012) 981–986.
[50] D. Guergova, E. Stoyanova, D. Stoychev, I. Avramova, P. Stefanov, Investigation of the inhibiting effect of cerium ions on the corrosion behavior of OC404 stainless steel in sulfuric acid medium, Open Chem. Phys. J. 4 (2012) 8–17.
[51] N. Wint, P. Ansell, J. Edy, G. Williams, H.N. McMurray, A method for quantifying the synergistic inhibitory effect of corrosion inhibitors when used in combination: a chromate generating coating, J. Electrochem. Soc. 166 (2019) C580–C588.
[52] B.M. Fan, G. Wei, Z. Zhang, N. Qiao, Characterization of a supramolecular complex based on octadecylamine and β-cyclodextrin and its corrosion inhibition properties in condensate water, Corros. Sci. 83 (2014) 75–85.
[53] S. Amiri, A. Rahimi, Preparation of supramolecular corrosion-inhibiting nanocontainers for self-protective hybrid nanocomposite coatings, J. Polym. Res. 21 (2014), 566(2-8).
[54] A. Altin, M. Rohwerder, A. Erbe, Cyclodextrins as carriers for organic corrosion inhibitors in organic coatings, J. Electrochem. Soc. 164 (2017) C128–C134.
[55] A. Altin, M. Krzywiecki, A. Sarfraz, C. Toparli, C. Laska, P. Kerger, A. Zeradjanin, K. J.J. Mayrhofer, M. Rohwerder, A. Erbe, Cyclodextrin inhibits zinc corrosion by destabilizing point defect formation in the oxide layer, Beilstein J. Nanotechnol. 9 (2018) 936–944.
[56] S. Szunerits, D.R. Walt, Aluminum surface corrosion and the mechanism of inhibitors using pH and metal ion selective imaging fiber bundles, Anal. Chem. 74 (2002) 886–894.